DRAGONWORX
BIOMIMETIC TECHNOLOGIES

August 2026 · Confidential · Richardson, Texas

AMRS – ADAPTIVE MERIDIAN RESONANCE SUIT

A self-powered therapeutic garment line for partial-mobility and neurological populations

AMRS: ADAPTIVE MERIDIAN RESONANCE SUIT

A self-powered therapeutic garment line for partial-mobility and neurological populations

> Every therapeutic wearable on the market today makes one of two trades. Either it is passive but dumb — a compression stocking, a knee brace, a heating pad — or it is smart but dependent, requiring daily charging, clinical supervision, or a five-figure price tag. AMRS refuses that trade. It harvests electrical energy from the wearer's own gait, routes that energy along the body's lowest-impedance tissue pathways, and delivers therapeutic electrical and vibrational stimulus continuously, all day, with no battery and no user compliance burden.

What This Does That Nothing Else Does

FOUR CAPABILITIES, NONE OF WHICH CURRENTLY COEXIST IN A SINGLE PRODUCT

- Self-powered therapeutic output. Triboelectric nanogenerators (TENGs) woven into high-flexion zones convert gait friction into usable current. Existing electrostimulation wearables (TENS units, NMES sleeves, the Quell device) all require batteries. AMRS delivers baseline therapy at zero charge state — eliminating the single largest failure mode in therapeutic wearables, which is that patients stop charging them.
- Dual-modality stimulation in one substrate. Electrical stimulation drives neuromuscular depolarization; low-frequency mechanical vibration drives fascial mechanotransduction. These are distinct tissue systems with distinct receptor populations. No commercial garment combines both. AMRS layers body-coupled electrical stimulation (BCES) and vibroacoustic therapy (VAT) transducers on a shared conductive network.
- Anatomically-routed current delivery. Electrodes are positioned along connective-tissue planes that exhibit measurably lower electrical impedance than surrounding tissue. Current self-routes along these low-resistance channels rather than diffusing isotropically from the electrode. This is the meridian alignment — explained below, and grounded in impedance spectroscopy, not tradition.
- Passive mechanical assist without actuators. Nacre-analog elastic laminates store energy at knee flexion and return it at toe-off. Variable-stiffness polymers stiffen under stance-phase load and relax during swing. This delivers a fraction of a powered exosuit's assist — but at 1/100th the cost, 1/10th the mass, and zero power draw.

On "Meridians" — What the Term Actually Refers To Here

Traditional Chinese Medicine maps roughly twenty pathways across the body surface along which it claims a vital energy circulates. Set aside the energetic claim entirely; it is not load-bearing for this design. What matters is that these pathways were empirically drawn over two millennia of clinical observation, and modern anatomical work has found that they correspond, with striking consistency, to real structures.

Langevin and Yandow (2002, The Anatomical Record) dissected the correspondence directly: roughly 80% of classical acupoints and 50% of mapped meridian segments coincide with intermuscular or intramuscular connective tissue planes — the fascial cleavage planes between adjacent muscles, or between muscle and bone. Ahn et al. (2005) then measured the electrical consequence: tissue impedance along meridian segments runs significantly lower than along parallel non-meridian control paths ($70.4 \pm 5.7\ \Omega$ vs. $75.0 \pm 5.9\ \Omega$), and the difference correlates with the presence of loose connective tissue visible on ultrasound.

> The operative reframe for a clinical reviewer: "Meridian" in this document should be read as a historically-derived empirical map of the fascial network's low-impedance conduction pathways. The map predates the instrumentation that validated it. We use it because it is the most complete such map in existence — not because we endorse the metaphysics originally attached to it.

This matters commercially as well as scientifically. The same map that provides an evidence-based electrode routing scheme also provides instant legibility in Asia-Pacific markets, where TCM framing drives an 18.3% CAGR in acupoint-stimulation devices — the fastest-growing regional segment in the category.

Market Structure and Revenue Potential

$18–22B	9.1%	1.4B	$400–1.8K
Aggregate addressable TAM, 2025 base	Blended CAGR across constituent markets	Global population aged 60+ (WHO)	Price tier with no incumbent occupant

SKU	COVERAGE	PRIMARY CLINICAL TARGETS	GLOBAL TAM	PRICE	YR-5 REV*
LW-1 Tights	Waist to toe	Sarcopenia, stroke gait rehab, Parkinson's, DVT, lymphedema, fall-risk reduction	$2.1B	$480–650	$34M
TW-1 Torso	Trunk, sleeveless	Chronic low back pain, fibromyalgia, osteoporosis, post-surgical recovery, scoliosis	$2.4B	$420–580	$29M
AC-1 Arm Cuff	Wrist to shoulder	Post-stroke hand rehab, carpal tunnel, RA, chemotherapy-induced neuropathy, CINV via PC6	$1.6B	$280–380	$22M
JK-1 Jacket	Waist up + arms	Adhesive capsulitis, MS upper-limb spasticity, Parkinson's rigidity, post-mastectomy lymphedema	$3.2B	$680–950	$41M
FS-1 Full Suit	Head to toe	Incomplete SCI, advanced MS, full-body stroke rehab, elderly independence maintenance	$5.8B	$1,200–1,800	$52M
HD-1 Crown	Head + cervical	Alzheimer's/dementia (40 Hz gamma), essential & Parkinsonian tremor, migraine, tinnitus, TBI, vagal dysregulation	$3.8B	$390–550	$47M
Aggregate (net of inter-SKU market overlap)			$18–22B	—	$225M

*Year-5 revenue models a 0.9–1.4% penetration of each SKU's serviceable obtainable market following Phase-2 clinical validation and Medicaid DME listing. Consumer on-ramp SKUs (MeridianSock $49, MeridianSleeve $129–189, ResonancePatch $89, AcuDrape Pro $449) are excluded from this table and modeled separately; they contribute an estimated additional $60–80M at Year 5 and serve primarily as ecosystem acquisition and real-world-evidence generation channels.

Evidence Base I — The Electrical Layer

The skeptical question is not whether transcutaneous electrical stimulation produces therapeutic effect; that is settled. The questions are (a) whether a garment can generate clinically meaningful current without a power source, and (b) whether anatomical routing improves on arbitrary electrode placement. Both have affirmative published answers.

Battery-free textile stimulation reaches muscle-activating field strengths

Full-textile body-coupled electrical stimulation (BCES) garments, powered solely by triboelectric conversion of movement and static charge, generate electric fields in the tens-to-hundreds of mV/mm range — sufficient to depolarize muscle fiber. In a controlled human trial, BCES socks produced a 21.47% increase in calf-raise frequency and a 6.25% reduction in muscle fatigue versus control, with no external power input whatsoever.

Wang et al. (2024), npj Flexible Electronics

TENG output falls within established therapeutic stimulation parameters

Triboelectric nanogenerators have demonstrated direct muscle stimulation at short-circuit currents as low as 35 μA — comfortably within transcutaneous safety envelopes and consistent with conventional NMES dosing. Critically, TENG output peaks at sub-5 Hz input frequencies, which is precisely the frequency band of human gait.

Wang et al. (2019), ACS Nano

Self-powered electrical patches accelerate tendon healing in vivo

TENG patches bonded to injured tendons, generating pulsed output from normal limb movement alone, produced significantly reduced inflammatory cell infiltration, increased collagen deposition, and complete tendon repair at 28 days versus incomplete repair in untreated controls. This establishes that motion-harvested current is not merely detectable but biologically consequential.

Park et al. (2023), Nano Energy

Piezoelectric-hydroxyapatite composites drive osteogenic differentiation

PVDF copolymer fibers loaded with hydroxyapatite nanoparticles show enhanced piezoelectric coefficient and demonstrated osteoblast differentiation in culture. This underpins the AMRS bone-adjacent fiber zones (tibia, hip, lumbar spine, sternum) as a candidate intervention for age-related and post-menopausal bone density loss — the upstream driver of the fragility fractures that terminate independent living.

Multiple; see reference list

Evidence Base II — The Vibroacoustic Layer

Vibroacoustic therapy (VAT) applies sinusoidal mechanical vibration in the 25–120 Hz band directly into soft tissue. Its clinical literature spans Parkinson's rigidity, MS spasticity, fibromyalgia pain, and stroke motor recovery. Its regulatory profile is favorable: FDA has determined vibroacoustic devices substantially equivalent to therapeutic vibrators and exempt from premarket notification.

Mechanical waves propagate measurably differently along meridian pathways

A hydrodynamic study applied 40 Hz vibration to pericardium-meridian points and adjacent control sites across 20 subjects. Mean wave transfer speed along the meridian was 4 m/s versus 8.5 m/s through control tissue, with significant differences in attenuation and peak amplitude as well. The tissue substrate of the pathway is physically distinct from surrounding muscle. Design consequence: a transducer at an acupoint does not radiate isotropically — it injects energy into a preferential propagation channel.

Chen et al. (2005), PMID 15673202

Meridian response appears frequency-specific, not broadband

Pilot work injecting sinusoidal signals across five frequencies into the Large Intestine meridian found significant propagation change at 7.8 Hz specifically — and not at adjacent test frequencies. If replicated, this implies meridian channels have resonant signatures rather than generic vibrational sensitivity, and that the AMRS frequency selector carries genuine therapeutic specificity rather than cosmetic user choice.

Reported in acupuncture electrophysiology literature; replication pending

40 Hz is independently privileged in two separate literatures

The MIT/Picower gamma-entrainment work (Iaccarino et al., Nature 2016) established that 40 Hz sensory stimulation attenuates amyloid load and modifies microglial state in murine Alzheimer's models, now advanced into human trials. Independently, 40 Hz is the probe frequency at which meridian wave-propagation asymmetry was demonstrated, and sits inside the 25–50 Hz band associated with bone density and tissue healing. This convergence was found, not designed — and it sets the AMRS default operating frequency.

Iaccarino et al. (2016), Nature 540:230–235

Transcutaneous vagal access is anatomically established

The auricular branch of the vagus nerve surfaces at the cavum conchae and is reachable non-invasively. Vibrational auricular stimulation produces measurable heart-rate-variability and autonomic-tone modulation. The HD-1 Crown combines mastoid bone-conduction (skull bone is a high-conductance, low-attenuation medium) with auricular and vertex nodes, targeting both the gamma-entrainment pathway and autonomic regulation in a single device.

Litscher et al. (2011), PMC3163402

Where the Evidence Is Thin — Stated Plainly

1. No head-to-head trial of VAT-at-acupoints versus electroacupuncture exists. The combination is mechanistically well-motivated — distinct receptor systems, distinct tissue targets — but the synergy is inferred, not demonstrated. This is a named Phase-1 study objective, and arguably a publishable result independent of commercial outcome.

2. Several recent trials show no superiority of electroacupuncture over sham for chronic pain. We regard this as informative rather than disqualifying: it suggests point-specificity may matter less than tissue-plane targeting for electrical modalities, which is consistent with our impedance-routing rationale and argues for the mechanical/fascial channel as the more specific of the two.

3. The 7.8 Hz resonance finding is pilot-scale and unreplicated. It is treated as a hypothesis to test, not a design foundation. AMRS therapeutic claims rest on the 40 Hz and BCES literature, both of which are substantially more mature.

4. Passive mechanical assist is real but modest. Nacre-laminate energy return will not restore gait to an individual who cannot generate it. AMRS is explicitly indicated for partial mobility loss — the population between "compression stocking" and "powered exosuit," which is where nearly all of the volume is.

Material Stack

Each layer solves a defined functional problem and traces to a biological mechanism already characterized in the materials literature. Several are shared with the DragonWorx Serpentis-class platform, spreading development cost across product lines.

Nacre-analog laminate Abalone shell brick-and-mortar	Alternating rigid platelet and compliant polymer layers store and return elastic strain energy at ~95% efficiency. Implemented as PVDF nanofiber laminate at knee and ankle: stores energy during stance-phase flexion, returns it at toe-off. Assist magnitude scales with gait velocity, so support is proportional to effort rather than constant.
Variable-stiffness dermis Sea cucumber mutable connective tissue	Holothurians modulate body-wall stiffness by an order of magnitude in under 100 ms via collagen cross-link state. The synthetic analog — cellulose nanocrystals in polyvinyl acetate — transitions on thermal, humidity, or voltage cue. At knee and hip it stiffens under stance load and relaxes at swing, replicating the dynamic stabilization that failing joint musculature no longer provides.
Helicoidal CFRP shell Mantis shrimp dactyl (Bouligand structure)	Rotating fiber ply schedule forces crack propagation into a helical rather than linear path, raising fracture energy ~70% at equal areal density. Deployed as low-profile patellar and greater-trochanter impact shells. Fall-related hip fracture is the dominant catastrophic event in this population, and conventional hip protectors fail on compliance because of bulk — which this geometry mitigates.
Shape-memory polymer elements Programmable geometry / 4D printing	Polyurethane SMP fibers hold a manufacturer-programmed corrected-posture geometry. Flexible at rest; as core temperature rises with activity, fibers migrate toward programmed shape, cueing lumbar lordosis and thoracic extension without rigid bracing. Recovery curve is tunable per-patient via the AI-guided geometry encoding developed for the Verdant Tower research thread.
PVDF triboelectric substrate Electric eel electrocyte stack (ElectraSuit lineage)	Knitted PVDF / silver-coated nylon composite serves simultaneously as energy harvester and stimulation distribution medium. Generates charge under both deformation (piezoelectric) and interlayer friction (triboelectric). Optimal harvest band coincides with normal gait frequency.
PVDF-hydroxyapatite fiber Native bone piezoelectricity / MICP biomineralization	Hydroxyapatite loading raises piezoelectric output while presenting a calcium-phosphate surface chemistry that mimics native bone matrix and guides osteoblast activity. Placed at bone-adjacent zones for localized osteogenic stimulus from ordinary daily movement.
Conductive meridian thread Ag-coated nylon / PEDOT:PSS	Silver-coated yarns (~1–5 Ω/cm) embroidered along mapped fascial-plane trajectories serve as both the BCES distribution network and the signal traces linking transducer nodes to the controller. Skin-contact zones use PEDOT:PSS for flexibility and biocompatibility; Ag/AgCl hydrogel pads snap off for independent laundering.
Miniature VAT transducers Vybronics VG0640001D / TDK PiezoHapt	6 mm diameter × 4 mm linear resonant actuators — the class of component shipping in consumer smartwatches — deliver Z-axis vibration normal to the skin. Wide-bandwidth variants (80 Hz resonant) cover the full 40–120 Hz therapeutic range. TDK PiezoHapt film at 0.35 mm adds distributed surface coverage at negligible bulk. All nodes under 8 g. Supply chain is mature and commodity-priced.

Regulatory Strategy

CLASS I / EXEMPT PATH — IMMEDIATE

LW-1, TW-1, and AC-1 in passive baseline configuration contain no powered stimulation circuit. They are compression garments with conductive thread that redistributes the wearer's own harvested charge. This positions them alongside compression hosiery rather than TENS units, avoiding 510(k) entirely. VAT-only configurations benefit separately from the FDA's substantial-equivalence determination exempting therapeutic vibrators from premarket notification.

CLASS II UPGRADE PATH — POST-EVIDENCE

App-controlled zonal activation introduces powered stimulation and likely triggers 21 CFR 882.5890 (transcutaneous electrical nerve stimulator) classification. Strategy is to ship passive first, accumulate real-world evidence through the consumer and clinic channels, then file 510(k) with post-market data in hand — inverting the usual sequence and materially de-risking the submission.

Go-to-Market Sequence

CHANNEL	ENTRY PRODUCT	RATIONALE	GATING REQUIREMENT
Practitioner clinics	AcuDrape Pro ($449) MeridianGlove Pro ($219)	Clinics already buy electrode patches, TENS units, and heat pads as consumables. A reusable instrumented drape displaces all three within existing purchasing behavior. No payer involvement.	None — revenue available pre-clinical
Direct consumer	MeridianSock ($49) MeridianSleeve ($129–189) ResonancePatch ($89)	Low-friction ecosystem on-ramp. Generates real-world usage and outcome data feeding trial design and 510(k) evidence. Likely FSA/HSA eligible.	Consumer-grade QMS only
Medicaid / DME	LW-1 Foundation ($380 MSRP)	Target reimbursement $220–260 via HCPCS A6xxx or L-code orthotic pathway. Highest-volume channel; needs fall-risk outcome data to secure listing.	Phase-2 RCT (n = 80, gait & fall endpoints)
Asia-Pacific	Full line, TCM-framed	18.3% regional CAGR in acupoint-stimulation devices. Meridian framing is an asset rather than a liability; several markets have shorter pathways than FDA.	Distribution partnership
Neuro / research	HD-1 Crown ($390–550)	Rides the NIH-funded 40 Hz gamma-entrainment pipeline. Investigator-initiated studies generate evidence at low company cost.	IRB-ready device build

Capital Plan

PHASE 1 — $1.2M

PVDF-HA fiber spinnability and wash-durability validation. TENG output characterization on human subjects across gait profiles. LRA node garment integration. LW-1 and AC-1 prototypes into IRB-approved feasibility study (n = 30, elderly partial-mobility cohort). Clinic channel soft launch.

PHASE 2 — $3.8M

Randomized LW-1 trial (n = 80) with gait velocity, TUG, and fall-frequency endpoints. Medicaid DME regulatory filing. AcuDrape Pro full clinic launch. HD-1 prototype into 40 Hz Alzheimer's pilot. First VAT-vs-electroacupuncture comparative study.

PHASE 3 — $8M+ (SERIES A)

FS-1 manufacturing scale-up. Asia-Pacific distribution partnership. IP portfolio build across the material stack. 510(k) submission for app-controlled SKUs supported by accumulated post-market data.

SELECTED REFERENCES

Langevin HM, Yandow JA (2002). Relationship of acupuncture points and meridians to connective tissue planes. The Anatomical Record 269(6):257–265.
Ahn AC et al. (2005). Electrical impedance along connective tissue planes associated with acupuncture meridians. BMC Complement Altern Med 5:10.
Chen et al. (2005). Hydrodynamic analysis of waveforms induced by vibrational stimuli at meridian and non-meridian points. PMID 15673202.
Wang et al. (2024). Full textile-based body-coupled electrical stimulation for wireless, battery-free wearable bioelectronics. npj Flexible Electronics.
Wang et al. (2019). Self-powered direct muscle stimulation using a triboelectric nanogenerator integrated with a flexible multiple-channel intramuscular electrode. ACS Nano.
Park et al. (2023). Self-powered wearable electrical stimulation patch with integrated TENG for tendinopathy treatment. Nano Energy.
Iaccarino HF et al. (2016). Gamma frequency entrainment attenuates amyloid load and modifies microglia. Nature 540:230–235.
Litscher G et al. (2011). Brain-modulated effects of auricular acupressure on autonomic function using vibration stimulation. PMC3163402.
Puhan MA et al. (2006). Didgeridoo playing as alternative treatment for obstructive sleep apnoea syndrome. BMJ 332:266.

Appendix A — Engineering Figures

Conceptual engineering drawings of the AMRS subsystem architecture. Reference numerals run in blocks of one hundred per figure and are consistent across the set. These are concept illustrations prepared for technical review, not manufacturing drawings; dimensions shown are target values rather than toleranced specifications.

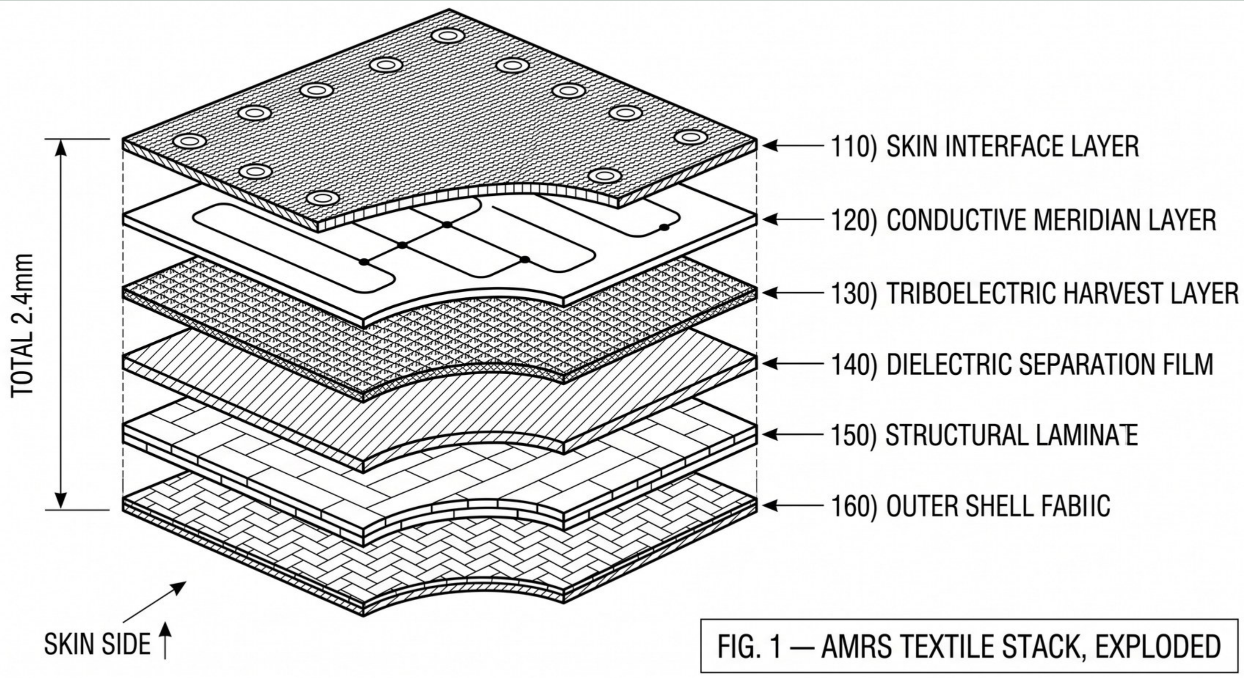

FIGURE 1 — AMRS TEXTILE STACK, EXPLODED

The six-layer garment substrate shown in exploded isometric, skin side uppermost. The skin interface layer (110) carries flush-mounted electrode contacts. The conductive meridian layer (120) routes silver-coated yarn in continuous serpentine paths with junction nodes at branch points. The triboelectric harvest layer (130) presents the micro-textured surface that generates charge against its counter-surface during flexion, separated from it by the dielectric film (140). The structural laminate (150) shows the offset brick-and-mortar platelet geometry derived from nacre, providing elastic energy return. The outer shell (160) is a conventional woven twill. Total assembled thickness 2.4 mm — within the range of ordinary performance compression wear.

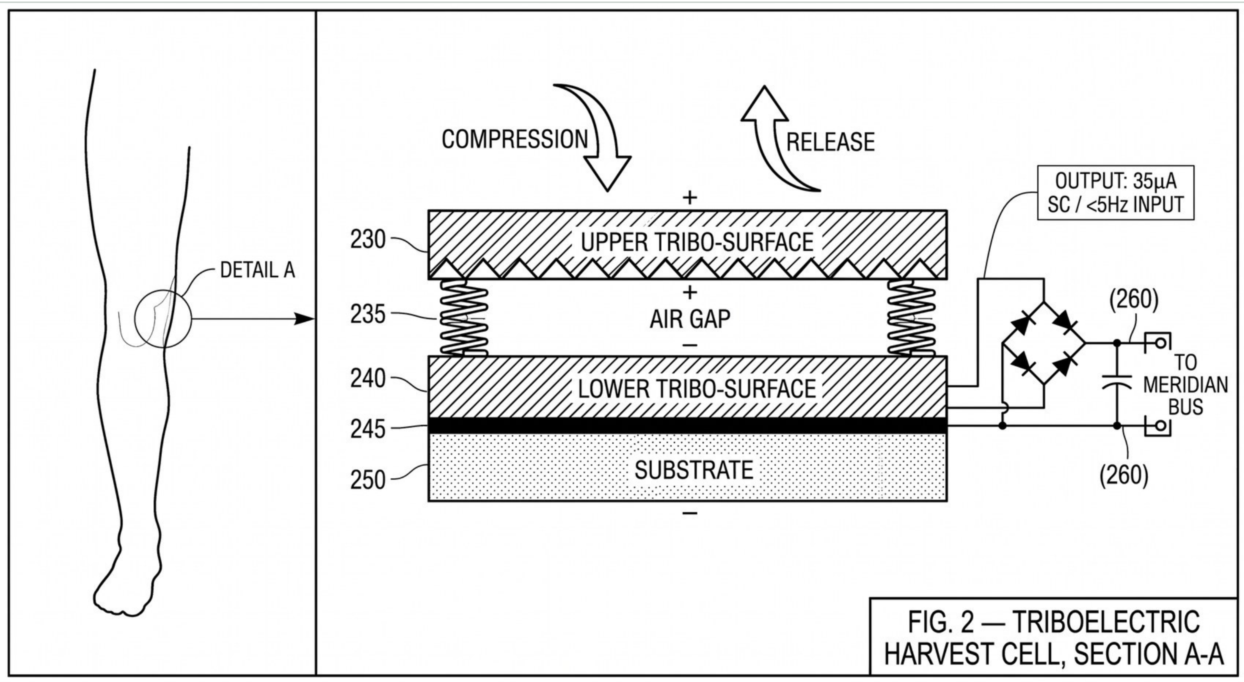

FIGURE 2 — TRIBOELECTRIC HARVEST CELL, SECTION A-A

Magnified cross-section of a single harvest cell, located at the lateral knee (Detail A, left panel). Under compression, the micro-pyramidal upper tribo-surface (230) contacts the lower tribo-surface (240) across the elastically-sprung air gap (235), driving contact electrification; on release, charge separation induces current in the electrode film (245). Output passes through a bridge rectifier to the storage capacitor (260) and onto the meridian bus. Characteristic output is 35 μA short-circuit at sub-5 Hz mechanical input — the frequency band of normal human gait.

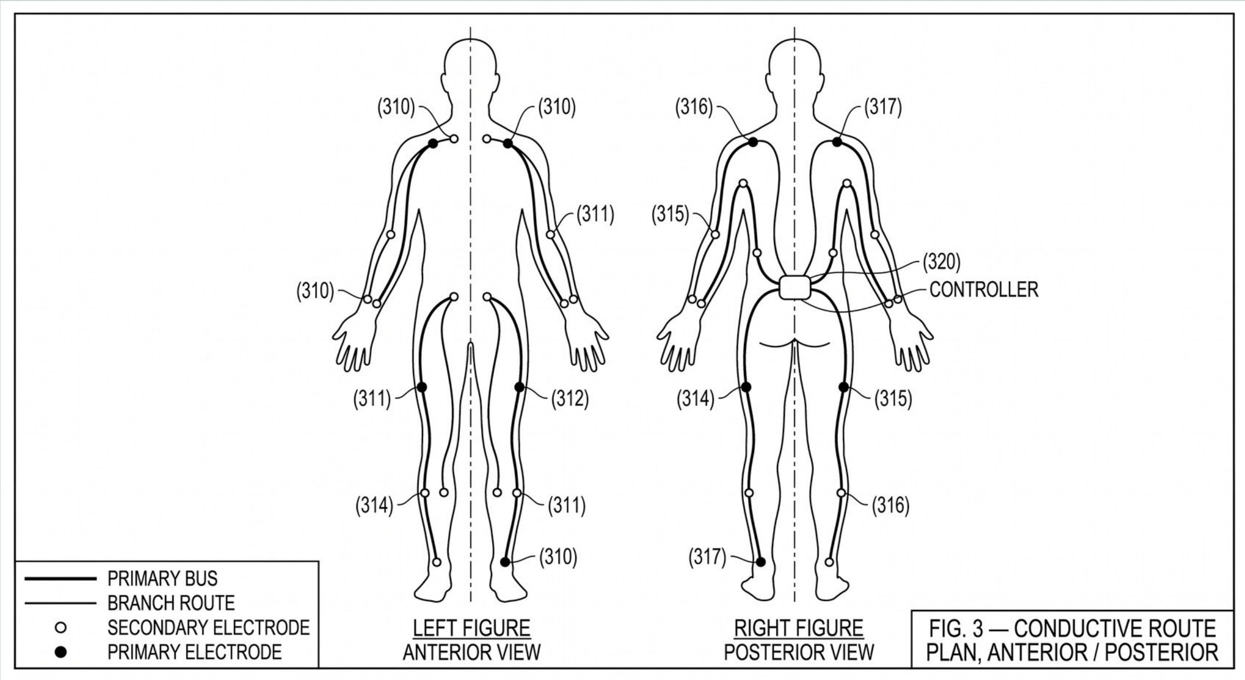

FIGURE 3 — CONDUCTIVE ROUTE PLAN, ANTERIOR / POSTERIOR

Full-body routing plan for the conductive network, shown in orthographic front and rear elevation. Heavy lines denote the primary bus; lighter lines denote branch routes. Open circles mark secondary electrodes; filled circles mark primary electrodes (310–317) positioned at the highest-influence points along each pathway. All routes converge at the controller medallion (320) at the lower back. Route geometry follows intermuscular and intramuscular connective-tissue planes, the anatomical substrate that classical meridian mapping empirically traces.

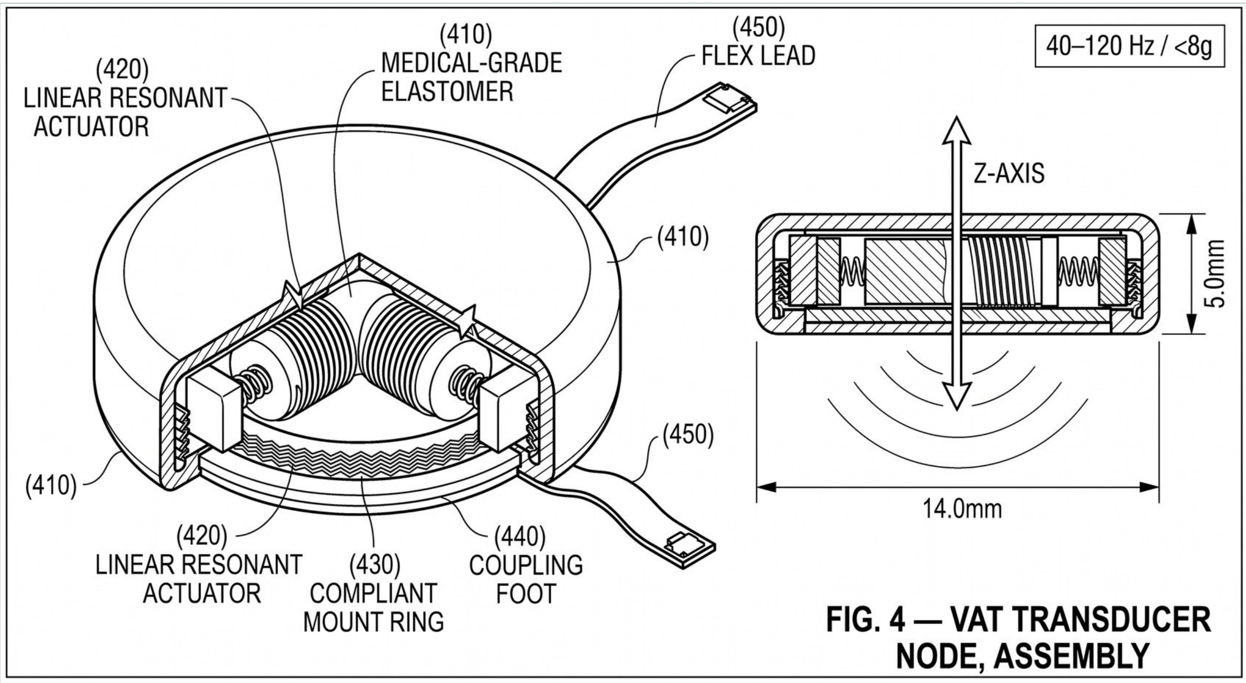

FIGURE 4 — VAT TRANSDUCER NODE, ASSEMBLY

The vibroacoustic transducer node in cutaway isometric (left) and straight section (right). A linear resonant actuator (420) is suspended within the medical-grade elastomer housing (410) on a compliant mount ring (430) that isolates the actuator from the housing shell and directs output downward through the coupling foot (440) into tissue. The flex lead (450) carries drive signal from the controller. Package envelope is 14.0 mm diameter × 5.0 mm, under 8 g, with usable output across the 40–120 Hz therapeutic band. Z-axis orientation places vibration normal to the skin surface.

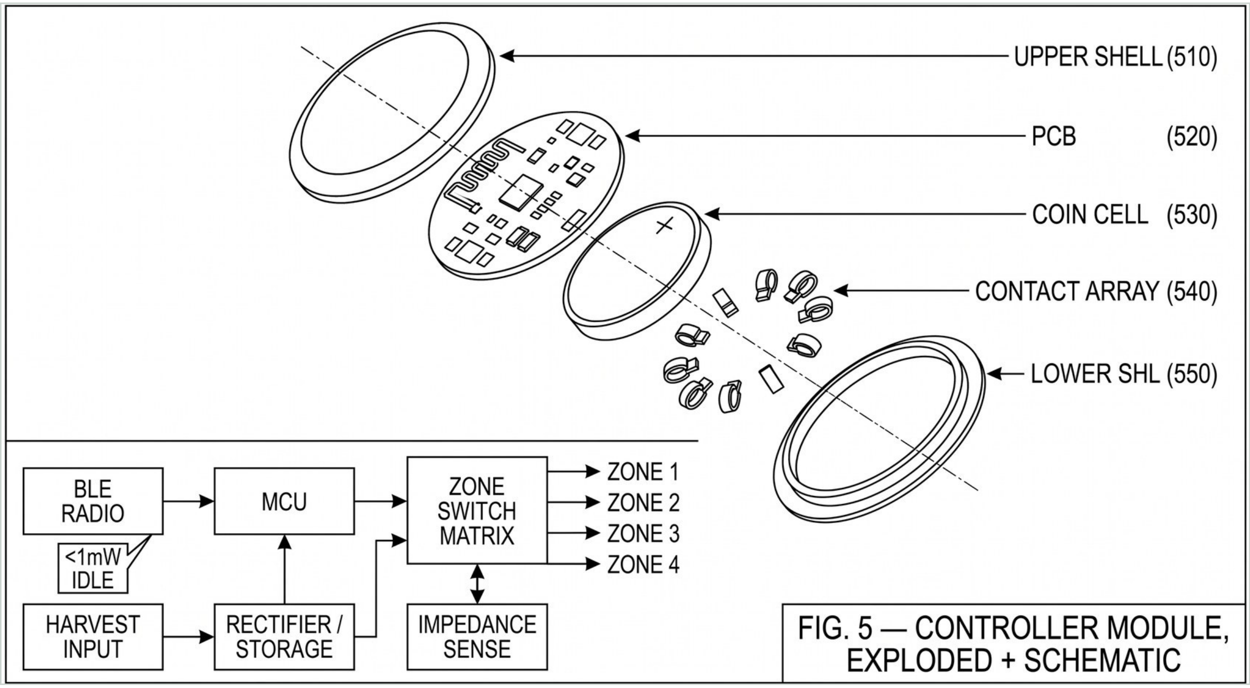

FIGURE 5 — CONTROLLER MODULE, EXPLODED + SCHEMATIC

The BLE controller medallion, shown exploded above its functional block diagram. Physical stack: upper shell (510), PCB (520) with integral meander antenna, coin cell (530), radial contact array (540) interfacing the garment's conductive network, and lower shell (550) with textile attachment flange. Functionally, harvest input feeds rectification and storage, which powers both the MCU and the zone switch matrix; the BLE radio receives zone-selection commands from the companion app at under 1 mW idle draw. Impedance sense provides closed-loop feedback on electrode contact quality. With no app connection, the module remains dormant and the garment operates passively.

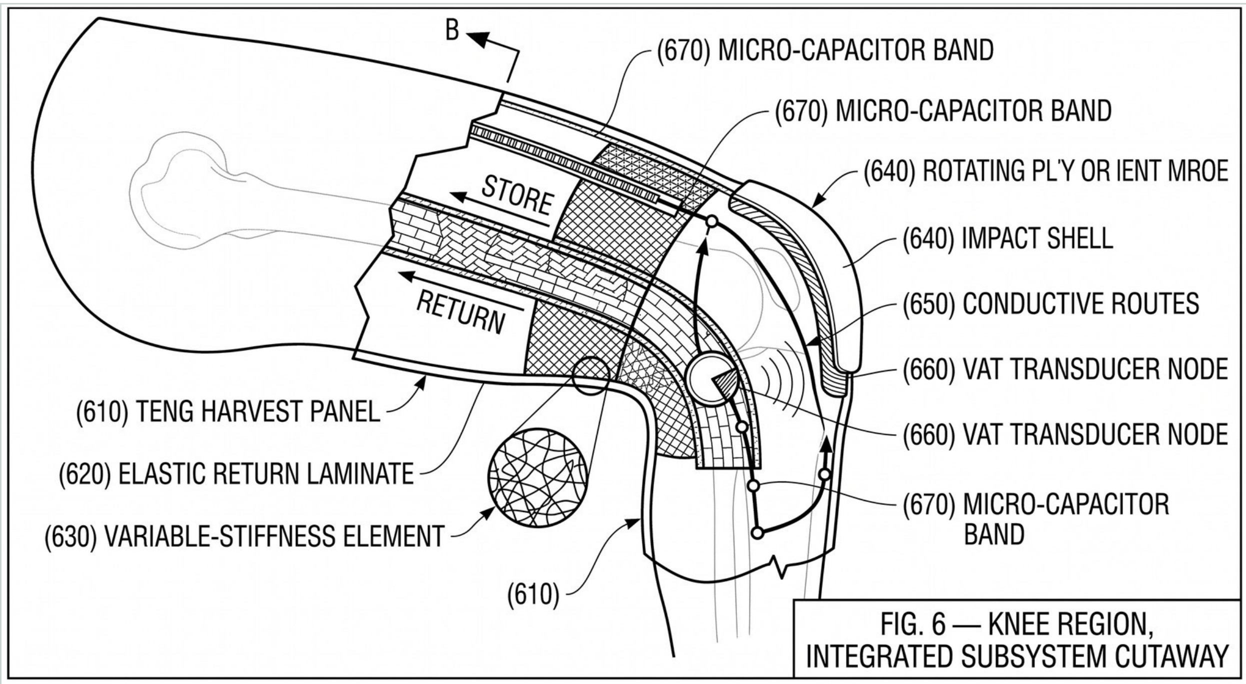

FIGURE 6 — KNEE REGION, INTEGRATED SUBSYSTEM CUTAWAY

All subsystems shown in situ at the knee, garment cut away over a phantom-line skeletal reference. The TENG harvest panel (610) sits over the lateral joint where flexion excursion is greatest. The elastic return laminate (620) spans thigh to calf, storing energy at flexion and returning it at toe-off. The variable-stiffness element (630) wraps the joint, its fiber network shown in the inset detail. The impact shell (640) over the patella displays the rotating ply schedule at its cut edge. Conductive routes (650) carry harvested charge upward (arrowheads) to the micro-capacitor band (670) at the upper thigh, while the VAT transducer node (660) radiates vibration inward toward the joint line.

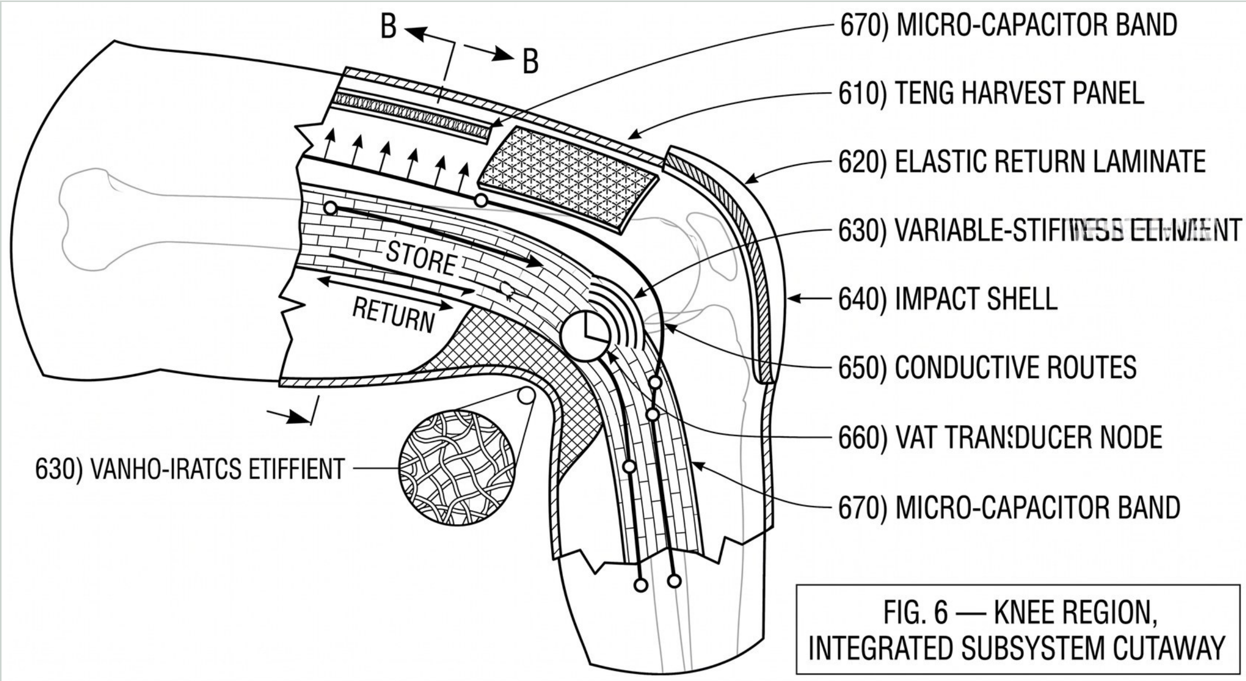

FIGURE 6A — KNEE REGION, ALTERNATE RENDERING

A second rendering of the same subsystem arrangement, retained for the clearer depiction of charge-migration flow along the conductive routes and the more legible separation between the elastic return laminate and the variable-stiffness element. Reference numerals match Figure 6. Several callout labels in both Figure 6 renderings contain generation artifacts and require correction before any external or filing use.